Switching the relaxation pathway by steric effects in conjugated dienes

Tateharu Tentaku,[1] Ryunosuke Atobe,[1] Takuro Tsutsumi,[2] Sota Satoh,[3] Yu Harabuchi,[2,4] Tetsuya Taketsugu,[2,4] and Taro Sekikawa[1]

[1] Department of Applied Physics, Hokkaido University, Sapporo 060-8628, Japan.
[2] Department of Chemistry, Faculty of Science, Hokkaido University, Sapporo 060-0810, Japan.
[3] Graduate School of Chemical Sciences and Engineering, Hokkaido University, Sapporo 060-0810, Japan.
[4] Institute for Chemical Reaction Design and Discovery (WPI-ICReDD), Hokkaido University, Sapporo, Hokkaido 001-0021, Japan.

E-mail: sekikawa@eng.hokudai.ac.jp

Received xxxxxx
Accepted for publication xxxxxx
Published xxxxxx

Abstract

Modification of a molecular structure at the minimum-energy conical intersection (MECI) on the relaxation pathway of the smallest conjugated polyene, *trans*-1,3-butadiene (BD), was achieved by substituting the hydrogen atoms at the end of the molecular chain with methyl groups. At the MECI between S_1 and S_0, BD is known to have a pyramidalized structure; therefore, the substituted methyl groups are expected to hinder this pyramidalization and change the relaxation pathway. Here, the relaxation dynamics of three conjugated dienes: BD, *trans*-1,3-pentadiene (PD), and 2,5-dimethyl-2,4-hexadiene (HD), were investigated by time-resolved photoelectron spectroscopy (TRPES) using single-order high harmonic pulses. Ultrafast relaxation to the ground state with decay times of less than 100 fs was observed in all three molecules. The potential energy curves from the theoretical calculation show the common features among these dienes, which explains the similar relaxation dynamics. However, HD was found theoretically to have a transoid structure at MECI between S_1 and S_0, while BD and PD both had pyramidalized structures. The relaxation pathway switching was corroborated experimentally by analysis of the photoelectron spectra specifically appearing in HD after a few hundred femtoseconds upon photoexcitation. The larger twist in the transoid structure stimulates molecular vibrations that modulated the photoionization probabilities.

1. Introduction

Conjugated polyenes are found in light-harvesting complexes as photon-capturing antennas for photosynthesis, and in rhodopsin for converting light into electrical signals in the vision system [1]. After photoabsorption, ultrafast energy transfer, conformational changes, and the conversion to thermal energy take place in conjugated polyenes and play important roles in biological systems. Therefore, the ultrafast processes in the conjugated polyenes upon photoexcitation are interesting issues from the viewpoint of time-resolved spectroscopy.

Among conjugated polyenes, we are interested in 1,3-butadiene (BD) because of its structural simplicity. BD has been investigated both experimentally and theoretically to understand energy relaxation processes in conjugated polyenes in a simplified manner [2-13]. In gaseous BD, the lowest optical excitation corresponds to the π→π* transition: the $1^1A_g \rightarrow 1^1B_u$ band, with a peak absorption of approximately 210 nm (5.90 eV) [3,14]. The lifetime of 1^1B_u was found to be less than 50 fs by time-resolved ionization spectroscopy using ultraviolet and infrared pulses [5,6]. Time-resolved photoelectron spectroscopy (TRPES) using high harmonic pulses made it possible to observe both the relaxation of the excited state and the recovery of the ground state. The lifetime of the excited state and the recovery time of the ground state were 55±8 and 70±8 fs, respectively [13].

The observed fast disappearance of the excited state is consistent with the nonfluorescent nature of BD [15]. To

understand this, the potential energy surfaces and the minimum-energy conical intersections (MECIs) were investigated theoretically [10,13]. The theoretical calculation revealed that there exist at least two CIs: one between 1^1B_u and 2^1A_g ($(S_2/S_1)_{MECI}$) that causes rapid decay of the 1^1B_u state to an optically dark state 2^1A_g, and the other between 2^1A_g and 1^1A_g ($(S_1/S_0)_{MECI}$). Through these CIs, ultrafast relaxation to the ground state takes place. Here, three MECIs, shown in Fig. 1, were found at $(S_1/S_0)_{MECI}$, where the twisted methylene unit (Me) is positively charged (Me^+) or negatively charged (Me^-), and a transoid form [10]. Among them, the contribution of Me^- to the population transferred to S_0 was 32%, while those of Me^+ and transoid forms were 20% and 5%, respectively [10].

The structural feature of Me^- is that the hydrogen atoms at one end of the molecule stick out of the molecular plane to form the pyramidalized structure, breaking the planarity of the molecule. This structural feature prompted the following questions: What will happen if the pyramidalization is restrained? Moreover, is it possible to change or to choose the contributing CI in the relaxation process? One approach to answer these questions is to investigate substitution effects. We have previously found that substitution effects change the dynamics of proton transfer in salicylideneaniline derivatives [16-18]. Now, if the hydrogen atoms at the end of the BD carbon chain are replaced with methyl groups, steric hindrance between the methyl groups is expected because the van der Waals radii of the hydrogen atom and the methyl group, by Pauling, are 0.12 and 0.2 nm, respectively [19]. The spatial interference between the methyl groups should raise the energy of Me^-. In addition, the mass effect and the electron affinity should also be considered, as discussed by Ichikawa and Takatsuka on the modification of CIs by the trifluoromethyl group [20]. The interplay among MECIs and the relaxation pathways are interesting issues.

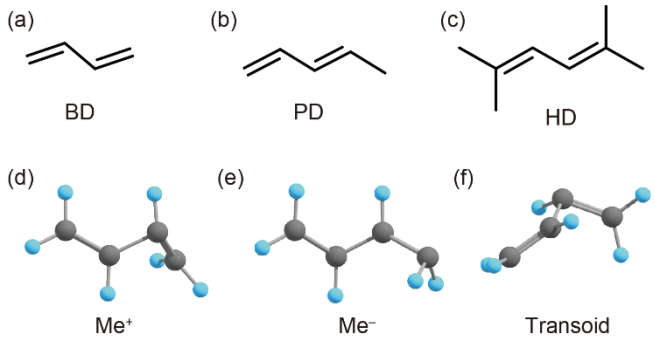

Fig. 1 Structural formulas of (a) BD, (b) PD, and (c) HD. Structural geometries of the three S_1/S_0 minimal energy MECIs of BD: (d) Me^+ MECI, (e) Me^- MECI, and (f) transoid MECI, which were reported in [10].

Therefore, in this work, we focused on the derivatives of BD and investigated the relaxation dynamics of 1,3-pentadiene (PD) and 2,5-dimethyl-2,4-hexadiene (HD) by TRPES, which were pumped at 400 nm (3.1 eV) in the two-photon excitation and probed by high harmonic pulses at 42.1 nm (29.5 eV) [21,22]; these are also compared with the previous results of BD [13]. In these derivatives, the hydrogen atoms located at the end of the carbon chain are replaced with methyl groups. However, they are still conjugated dienes; therefore, their electronic structures in the ground state are almost identical to that of BD. The relaxation dynamics of HD, with complete methyl substitution, should reflect the steric effects, whereas that of PD, in which one end of the carbon chain can still be pyramidalized [20], is expected to be similar to that of BD.

2. Experimental setup and computational details

The detail of the experimental setup has been described elsewhere [23]. Briefly, we used a Ti:sapphire laser system delivering 800-nm, 1.1-mJ, 30-fs pulses at a repetition rate of 1 kHz for TRPES. After the second harmonic generation by a LiB_3O_5 (LBO) crystal (500 μm thickness) for the pump pulses with a pulse energy of 40 μJ, the remaining fundamental pulses were focused into a Kr pulse gas jet for high harmonic generation. The 19th harmonic (29.5 eV) for the probe was selected among many harmonics by a time-delay compensated monochromator (TDCM) [21,22,24-26], enabling the single harmonic selection with the time duration preserved. A TDCM consists of a pair of toroidal gratings and a slit: the first grating and the slit select the harmonic order and the second grating compensates for the pulse front tilt caused by the diffraction on the first grating. The shortest pulse duration of the selected high harmonics achieved in our system was 11 fs [21]. The samples were excited by 400-nm photons in the two-photon excitation. Because of the symmetry of the molecular structure, HD was pumped only to 2^1A_g, while PD might be pumped to other states due to the symmetry breaking. The energy of the pump pulse was reduced to less than 14 μJ, which was the minimum energy necessary to observe the signals of the excited states and prevent excitation to higher states. The energy was reduced by the attenuator composed of a pair of thin film polarizers and a half-wave plate. Both the pump and probe pulses were focused into the sample gas with a polarization angle of 55° to avoid the time dependence induced by molecular rotation. The photon flux on target was ~10^9 photons/s, corresponding to a pulse energy of 5 pJ [22].

PD and HD were purchased from Tokyo Chemical Industry and used without any further purification. The sample gas at room temperature for PD and warmed at 313 K for HD was guided to the entrance of a magnetic bottle time-of-flight photoelectron spectrometer through a copper pipe. The retardation electric field was applied in the flight tube to improve the spectral resolution of the spectrometer. The transient photoelectron spectra were recorded by changing

the optical delay between the pump and probe pulses. The temporal evolution of the photoelectrons ejected by the two-photon ionization of Kr gas by pump and probe pulses, that is, the cross-correlation function [27], was employed as the response function of the system, of which the width τ_{FWHM} was 77 fs. Since we have already optimized the diffraction angle of the grating in the TDCM [21], the temporal width was mainly limited by the pump pulse duration.

For theoretical investigation of the excited-state dynamics of PD and HD, reaction pathways (meta-intrinsic reaction coordinates (meta-IRCs)) were calculated from the Franck-Condon (FC) structure in the 2^1A_g state using the multi-reference second-order perturbation theory (CASPT2) [28]: multi-state (MS-) CASPT2 with three singlet states mixed together was used for PD, and single-state (SS-) CASPT2 was used for HD. The ionization energy was calculated at the CASPT2 level along the meta-IRC in the 2^1A_g state as the energy difference between the 2^1A_g state of the neutral species and the three lowest doublet states of the cationic species. We also optimized the MECI between 2^1A_g and 1^1A_g ($(S_1/S_0)_{MECI}$) to investigate the ground state relaxation process. Recently, the $(S_1/S_0)_{MECI}$ structure has been thoroughly investigated for BD using the GRRM program [29]. To obtain the geometrical structure of $(S_1/S_0)_{MECI}$, a preliminary search was performed at the spin-flip time-dependent density functional theory (SF-TDDFT) [30] level by the gradient projection/single component (SC)-artificial force induced reaction (AFIR) method [31], followed by optimization of the $(S_1/S_0)_{MECI}$ structure [32-34] at the CASPT2 level.

Meta-IRC calculations and MECI optimization were performed using the GRRM17 program [35] SF-TDDFT calculations were performed with GAMESS [36] using the BHHLYP functional and the 6-31G(d) basis set; CASPT2 calculations were performed with MOLPRO2012 [37] using the cc-pVDZ basis set. In CASPT2, the state-averaged complete active space self-consistent field (SA-CASSCF) wavefunction [38,39] was used as the reference function, with S_0, S_1, and S_2 states averaged, and four electrons and four orbitals as the active space.

3. Results and discussion

3.1 Time-resolved photoelectron spectroscopy

Figures 2a and 2b show the photoelectron spectrograms of PD and HD, respectively. We found the following two features in the spectrograms. One is the small short-lived signals with ionization energies lower than the energy level of the highest occupied molecular orbital (HOMO) around 8 eV, that is, excited states, at delay times of around 0 fs. The other is the decrease in the photoelectron intensity between 11 and 15 eV in HD up to 1 ps upon photoexcitation, while only small changes were observed in PD. These intensity changes are recognized more clearly in the time-resolved photoelectron spectra shown in Figs. 2c and 2d for PD and HD, respectively.

In the case of BD [13], the temporal behavior was similar to that of PD: while the ultrafast relaxation of the excited state was observed, the changes in the photoelectron spectrum, which is induced by the antisymmetric C=C stretching mode stimulated after returning to the ground state, was less significant than those of HD. These features indicate that the methyl group substitution effects in PD are minor for the relaxation dynamics. Relatively larger changes in the HD spectra are noteworthy.

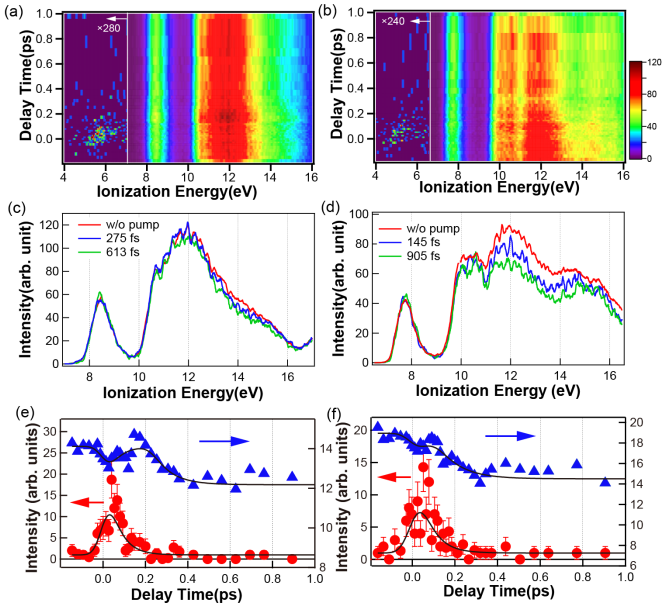

Fig. 2 Photoelectron spectrograms of (a) PD and (b) HD. (c) Time-resolved photoelectron spectra of PD before pump (red), at 275 fs (blue), and at 613 fs (green). (d) Time-resolved photoelectron spectra of HD before pump (red), at 145 fs (blue), and at 905 fs (green). (e) Time dependences of PD photoelectron yields between 5.48 and 6.59 eV (●) and between 12.05 and 15.17 eV (▲). (f) Time dependences of HD photoelectron yields between 4.31 and 6.22 eV (●) and between 11.09 and 13.42 eV (▲). The solid lines in (e-f) are the fitted results.

Here, we would like to focus on the dynamics of the excited states. The short-lived signals were also observed in BD with a lifetime of 55±8 fs, suggesting the decay component from the FC state of 2^1A_g in comparison with the theoretical calculation [13]. Because the electronic structures of PD and HD, in particular the HOMO, primarily come from the electron conjugation on the carbon chain like in BD, the observed short-lived excited states could be attributed to the FC states upon photoexcitation, which will be confirmed theoretically later.

To see the relaxation dynamics from the FC states, the time dependencies of the photoelectron intensities integrated between 5.48 and 6.59 eV for PD and between 4.31 and 6.22 eV for HD are shown by circles in Figs. 2e and 2f, respectively. The decay time τ_1 of the photoelectron intensity was obtained by the least-squares fitting of the data to the exponential function $I(t)=\exp(-t/\tau_1)$ convoluted with the correlation function $R(t)=\exp\{-4\ \ln 2\ (t/\tau_{FWHM})^2\}$, where t is the time and τ_{FWHM} = 77 fs. The fitting function $f(t)$ is expressed as

$$f(t) = A\int_{-\infty}^{t} R(t')I(t-t')\,dt', \quad (1)$$

where A is the amplitude. The fitting results are shown by the solid lines in Figs. 2e and 2f with lifetimes of 56±12 fs and 64±16 fs for PD and HD, respectively. These values are very close to that of BD. Contrary to the expectation that the methyl groups hinder the terminal-carbon atom pyramidalization, the substitution effects on the decay dynamics from the FC states in HD were not notable.

3.2 Reaction path in the excited states

Figure 3 shows the potential energy curves (PECs) of the S_0, S_1, and S_2 states of the neutral species and the D_0 and D_1 states of the cationic species for PD and HD along the meta-IRC pathways, starting from the FC structures in the S_2 (2^1A_g) state. In both PD and HD, the energy level of the doubly excited $\pi^2\pi^{*2}$ state (2^1A_g) is slightly higher than that of the $\pi\pi^*$ state (1^1B_u) at the FC structure, and the crossing region between the S_2 and S_1 states appears immediately. As a result, the electronic structure of the S_1 state changes into the doubly excited state after the crossing region. Therefore, when excited into the 2^1A_g state by two photons at the FC structure, the molecule quickly relaxes from the S_2 state to the S_1 state, and since there is no barrier, it smoothly reaches the $(S_1/S_0)_{CI}$ region to return to the ground state. The features of the PD and HD relaxation dynamics are similar to those of BD [13], where these molecules have very short lifetimes in the excited states.

At the terminal point of the meta-IRC, the S_0 and S_1 states are almost degenerate, corresponding to the CI. In Fig. 3, the $(S_1/S_0)_{MECI}$ with the lowest energy is plotted next to the terminal of the meta-IRC. Here, we discuss the geometrical structure of $(S_1/S_0)_{MECI}$ for PD and HD. In the search for $(S_1/S_0)_{MECI}$ at the SF-TDDFT level, $(S_1/S_0)_{MECI}$ structures with bond recombination and *cis-trans* isomerization were also obtained, but these are beyond the scope of discussion because they are far from the FC region of the *trans*-form. The $(S_1/S_0)_{MECI}$ structures related to the *trans*-form of PD and HD can be classified based on the carbon atoms where the deformation of the twisted-pyramidal geometry occurs. In the case of PD, the diene has four carbon atoms, but in the case of HD, there are two independent carbon atoms due to symmetry. By performing a $(S_1/S_0)_{MECI}$ search from the FC region, all six types of structures were successfully obtained. In Fig. 4, the structures and energies of the low-energy $(S_1/S_0)_{MECI}$ optimized at the CASPT2 level are shown. The four structures for PD are shown in Figs. 4a–4d, and the two structures for HD are shown in Fig. 4e–4f.

The most stable $(S_1/S_0)_{MECI}$ structure obtained for PD is the CH_2 terminal pyramidal form, in which the pair of hydrogen atoms of the terminal carbon atom without a methyl group is located off the molecular plane (Fig. 4a). This CH_2-pyramidal form is not affected by methyl substitution, like in BD. The energy difference between this MECI and the S_1 minimum is very small; furthermore, the meta-IRC starting from this MECI reaches the S_1 minimum without any energy barrier. Therefore, it is postulated that PD entering the S_1 minimum region decays rapidly to the ground state *via* the CH_2-pyramidal CI. This mechanism is consistent with that of BD [13], and supports the experimental ultrafast relaxation process of PD. Note that the energy differences of the other MECIs shown in Figs. 4b–d are small, but the meta-IRC from these MECIs does not reach the S_1 minimum in Fig. 3. In the case of HD, the transoid form with twisted carbon chains (Fig. 4e) is more stable than the pyramidal form with CH_2 terminals (Fig. 4f). Furthermore, the energy difference between the meta-IRC terminal structure (shown in Fig. 3d) and the transoid-CI is almost zero. This difference (between PD and HD) can be understood with regard to the steric effect of the methyl substituent. By substituting all four hydrogen atoms on the terminal carbon of BD, the CI with the accompanying geometrical deformation around the terminal carbon atom became unstable. Thus, the present calculations indicate that although the decay mechanisms of PD and HD are different, both molecules exhibit ultrafast decay.

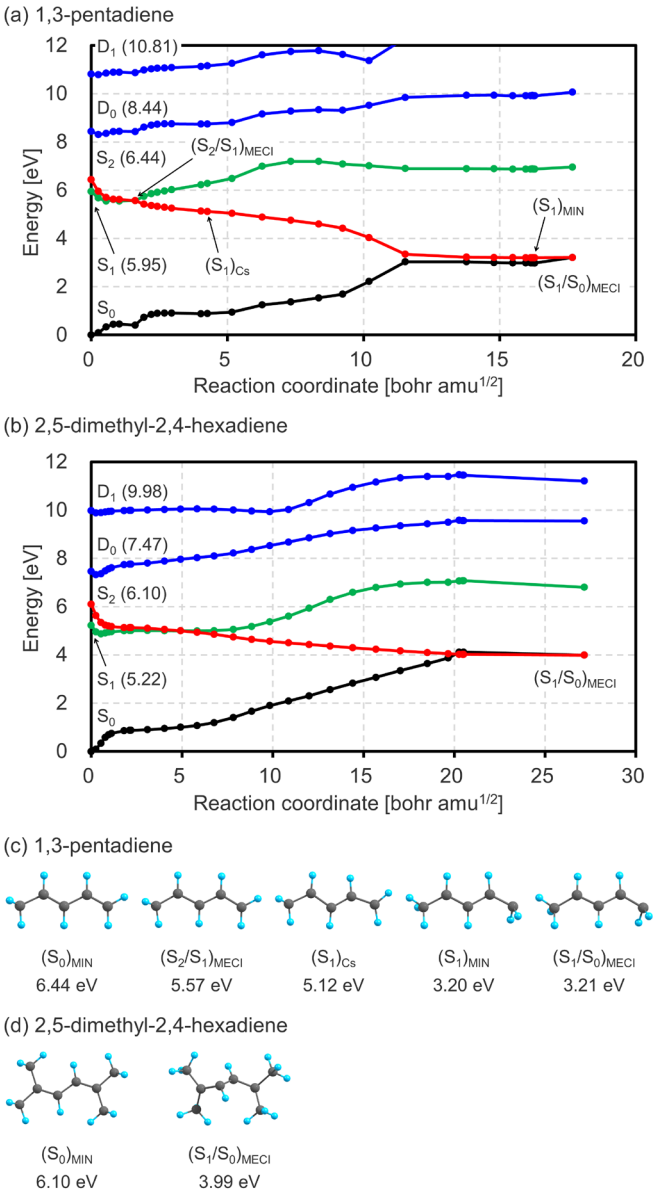

Fig. 3 Potential energy curves (PECs) of the S_0, S_1, and S_2 states of the neutral species and the D_0 and D_1 states of the cationic species for (a) PD and (b) HD along the meta-IRC pathways, starting from the FC structures in the S_2 (2^1A_g) state. The red, green, black, and two blue curves denote the potential energy for the doubly excited state (2^1A_g), the ππ* state (1^1B_u), the ground state (1^1A_g) of the neutral species, and the ground state (D_0) and the first excited state (D_1) of the cationic species, respectively. The key structures along the meta-IRC paths: (c) $(S_0)_{MIN}$, $(S_2/S_1)_{MECI}$, $(S_1)_{Cs}$, $(S_1)_{MIN}$, and $(S_1/S_0)_{MECI}$ for PD and (d) $(S_0)_{MIN}$ and $(S_1/S_0)_{MECI}$ for HD are shown. The energies of the 2^1A_g state relative to the ground state are also shown for the respective structures.

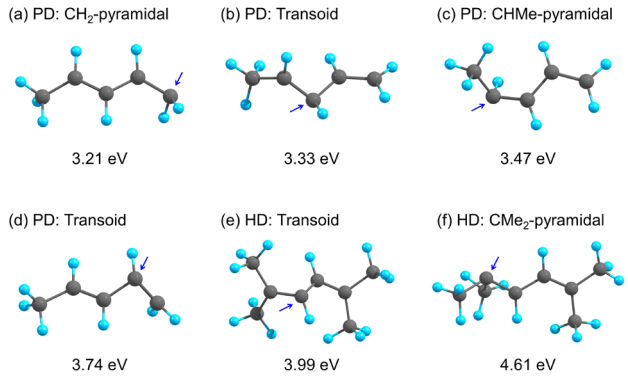

Fig. 4 (a-d) Low-energy $(S_1/S_0)_{MECI}$ structures of PD determined at the MS-CASPT2 level and (e, f) Low-energy $(S_1/S_0)_{MECI}$ structures of HD determined at the SS-CASPT2 level. For each structure, the relative energy is shown at which the ground state minimum at $(S_0)_{MIN}$ is zero. Pyramidalized or twisted carbon atoms are indicated by blue arrows.

3.3 Ultrafast dynamics from the Franck-Condon structure to conical intersections

In 3.1, we showed the relaxation dynamics by integrating the whole signals from the excited states. Spectrally resolved signals, however, provide us more opportunities to gain insight into the relaxation processes from the FC structure. The spectrograms shown in Fig. 5a and 5c are the magnified spectrograms of PD and HD, respectively, and were analyzed to closely examine the signals from the excited states. To compare with the PEC of PD, the vertical ionization energies of the key structures on the PEC to the ground state (D_0), the first excited state (D_1), and the second excited state (D_2) of the cation were calculated and are summarized in Table 1.

We divided the spectrum region (shown in Fig. 5a) into three and denoted them as I, II, and III. The signal in region I appeared only around time zero. The time-integrated spectra between −66.7 and 13.2 fs have a peak at 5.34 eV, shown by the red line in Fig. 5b. This peak should originate from two processes. One is the two-photon ionization of the HOMO to D_0 by 400 nm and probe photons; that is, the cross correlation, because the peak energy shifts from the HOMO at 8.48 eV, shown by the green line in Fig. 5b, by 3.11 eV. The other is the ionization from $(S_2/S_1)_{MECI}$ to D_1 with an energy of 5.29 eV (shown in Table 1). In both processes, the peak in region I is expected to appear immediately upon photoexcitation.

The blue line in Fig. 5b is the spectrum integrated between 26.5 and 119.8 fs, which has two peaks at 5.60 eV and approximately 6.5 eV in region II and III, respectively. The appearance of the photoelectrons in regions II and III were delayed from time zero by 27 and 40 fs, respectively. This suggests that the peak at 5.60 eV comes from the relaxing state from the FC state, and the band in region III arises from

further deactivation. However, in region II, the signals were observed up to 100 fs, comparable to region III. Thus, the peak at 5.60 eV should come from a relatively stable state. Focusing on the structural changes along the meta-IRC from the FC structure, after $(S_1)_{Cs}$, the molecular structure changes from an in-plane motion with the C_s symmetry to an out-of-plane motion, which leads to the CH_2-terminal pyramidalization. Thus, the molecule descending the meta-IRC restricted in the C_s symmetry should stay around the $(S_1)_{Cs}$ region because of the mismatch between the molecular momenta and the direction proceeding to the out-of-plane motion. The S_1-D_1 transition energies along the meta-IRC related to the in-plane motion are within 5.57–6.04 eV (See Fig. 3a and Table 1), corresponding to the peak energy in region II (5.60 eV). Therefore, region II can be assigned to the structural changes keeping with the C_s symmetry in the S_1 state.

The photoelectrons in region III appeared later than in region II and were shifted toward higher ionization energy with time. The time-integrated spectrum (shown by the blue line in Fig. 5b) extends to a higher ionization energy, compared with the earlier spectrum (shown by the red line). Therefore, the observed time-energy map corresponds to the temporal evolution of the nuclear wave packet on the S_1 state. Because the S_1-D_0 transition energy around $(S_1/S_0)_{MECI}$ on the PEC is 6.85 eV shown in Table 1, the peak in region III is attributable to $(S_1/S_0)_{MECI}$ and $(S_1)_{MIN}$. Further relaxation dynamics to the ground state were not observed, which might be due to the poor FC overlap.

In the case of HD, although the signal to noise ratio was poor for detailed analysis, the photoelectrons from the excited states appeared to shift to higher ionization energy with time. Analysis of the time-integrated spectra shown in Fig. 5d indicates that the peak at 5.4 eV (shown by the blue line) appeared delayed compared to the peak at 5.0 eV (shown by the red line). These peak energies are within the transition energies between S_1-D_1 and S_1-D_0 shown by the PECs in Fig. 3c and the dynamics is explained in the same manner as PD. Therefore, the initial relaxation process in HD and PD are similar, although the molecular structures at $(S_1/S_0)_{MECI}$ are different.

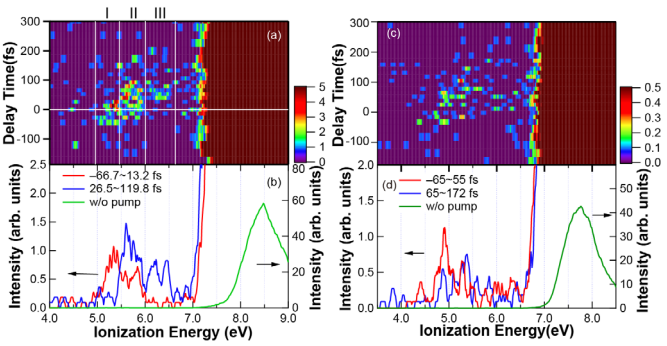

Fig. 5 (a) Photoelectron spectrogram of PD. The vertical white lines indicate the energy regions I, II, and III. The horizontal white line is time zero. (b) Time-resolved photoelectron spectra of PD before pump (green), integrated between −66.7 and 13.2 fs (red), and integrated between 26.5 and 119.8 fs (blue). (c) Photoelectron spectrogram of HD. (d) Time-resolved photoelectron spectra of HD before pump (green), integrated between −65 and 55 fs (red), and integrated between 65 and 172 fs (blue).

Table 1. Theoretical vertical transition energies (in eV) from the 2^1A_g state to the D_0, D_1, and D_2 states: the ground state, the first excited state, and the second excited state of the PD cation, respectively. $(S_0)_{MIN}$, $(S_2/S_1)_{MECI}$, $(S_1)_{Cs}$, and $(S_1/S_0)_{MECI}$ are named in the same way as in Fig. 3.

	$(S_0)_{MIN}$	$(S_2/S_1)_{MECI}$	$(S_1)_{Cs}$	$(S_1/S_0)_{MECI}$
D_0	2.49	2.86	3.63	6.85
D_1	4.87	5.29	6.04	9.76
D_2	7.00	6.68	7.32	11.17

3.4 Substitution effects on the low-lying molecular orbitals

After several hundred femtoseconds, a larger decrease in the HD photoelectron intensity around 12–14 eV was observed, while the spectral changes in BD [13] and PD were smaller (Figs. 2c and 2d). The triangles in Figs. 2e and 2f represent the time dependence of the photoelectron yield between 12.05 and 15.17 eV in PD and that between 11.09 and 13.42 eV in HD, respectively. These bands mostly arise from the MOs, which form σ bonds. Although the decrease in the photoelectron yield of PD is smaller than that of HD, the temporal behaviors are similar in these two molecules. Just after excitation, the photoelectron yield reduced on the same timescales as the excited-state dynamics shown in Figs. 2e and 2f. Hence, the initial reduction is attributed to the depletion and recovery of the ground state. Subsequently, the photoelectron yields decreased gradually. Because no significant peak shifts were observed in the photoelectron spectra, it is inferred that these molecules did not isomerize to other molecules within 1 ps. Therefore, we attribute these processes to vibrational equilibration after relaxation to the ground state i.e. vibrational relaxation. A certain period of time is required to distribute the absorbed photon energy (6.2 eV) among the vibrational modes. In the highly excited vibrational states, the Franck-Condon factors are different from those in the ground state, leading to a decrease in the photoelectron yield.

To evaluate the time for vibrational equilibration upon photoexcitation, the temporal evolutions of the lower-lying MOs are represented by the function $g(t)$, which is expressed as follows:

$$g(t) = N - A\int_{-\infty}^{t} R(t')I(t-t')dt' - B\int_{-\infty}^{t-\tau_{delay}} R(t')\left\{1 - H\left(t-t'-\tau_{delay}\right)\right\}dt' \quad , \quad (2)$$

where $H(t)=\exp(-t/\tau_2)$ and τ_2 is the time constant for vibrational equilibration. N, A, and B are amplitudes, and τ_{dealy} is the start time of vibrational equilibration. In Eq. 2, the second term represents pump depletion and relaxation to the ground state with a time constant of τ_1. Therefore, the value obtained by the fitting to the excited-state dynamics described in 3.1 is employed for τ_1. The third term expresses vibrational relaxation. The experimental data were fitted with $g(t)$ by the least squares method, and the results are denoted in Figs. 2e and 2f by solid lines. The obtained parameters are tabulated (Table 2).

Table2. Fitting results.

	τ_1 (fs)	τ_2 (fs)	τ_{dealy} (fs)
PD	56 ± 12	83 ± 2	219± 10
HD	64 ± 16	98 ± 7	97± 5

In addition to the larger decrease in the photoelectron yields of lower-lying MOs in HD, the τ_{delay} of HD is less than half that of PD, while the differences in τ_1 and τ_2 are not as significant. Totally, in HD, vibrational equilibrium was reached earlier than in PD. We believe that the relatively larger spectral changes and faster vibrational equilibration in HD are attributable to the structure at $(S_1/S_0)_{MECI}$. Considering the structures at $(S_1/S_0)_{MECI}$ and the corresponding PECs of these three molecules, the difference among them is the molecular structures at $(S_1/S_0)_{MECI}$, in that only HD has a transoid structure. The photoexcitation and rapid relaxation to the ground state induce molecular vibrations through structural changes in the excited states [40,41]. Because the main carbon chain in the transoid structure is twisted differently from that in the pyramidal one (Fig. 4), the stimulated vibrational modes in HD are different from those in PD and in BD. Considering the larger spectral changes in HD, the vibronic interaction with the stimulated vibrational modes upon photoexcitation is stronger in HD than in the others. This also indicates that the energy redistribution among the vibrational modes in HD occurs more rapidly. Hence, the τ_2 of HD can be smaller than that of PD.

Conclusions

We have investigated the substitution effects on the ultrafast relaxation processes in BD, PD, and HD by TRPES. In BD, the structure at the MECI between S_1 and S_0 is known to have a pyramidal structure, in which the hydrogen atoms at the terminal carbon atom stick out from the molecular plane. The methyl group substitution in PD and HD was expected to change the structure at the MECI because of the steric hindrance and the mass effect. However, the observed ultrafast dynamics earlier than several hundred femtoseconds were similar among the three compounds. Quantum chemical calculation predicts that the PECs are very similar and, therefore, ultrafast relaxation to the ground state was observed among all three molecules, although the key structure at the MECI of HD was different from those of BD and PD because of the steric hindrance of the methyl groups. The substitution effects manifest as the photoelectron spectra changes after several hundred femtoseconds upon photoexcitation in HD. The switching of the relaxation pathway from the pyramidal structure to the transoid structure in HD should lead to nonlinear photoexcitation dynamics, breather, in the longer polyene chains [42,43].

Acknowledgements

We thank Ryuji Itakura and Hiroshi Akagi for valuable discussion. TS is financially supported by MEXT Q-LEAP (JPMXS0118068681), JST CREST (JPMJCR15N1), and KAKENHI(19H01814). Tetsuya Taketsugu thanks to a grant from the Photo-excitonix Project in Hokkaido University and JST CREST (JPMJCR1902). Some of calculations were performed using the Research Center for Computational Science, Okazaki, Japan.

References

[1] Voet D and Voet J G, *Biochemistry* (John Wiley & Sons, 2010), 4th edn.
[2] Chadwick R R, Gerrity D P, and Hudson B S 1985 Chem. Phys. Lett. **115** 24-8.
[3] Mcdiarmid R and Sheybani A-H 1988 J. Chem. Phys. **89** 1255-61.
[4] Ito M and Ohmine I 1997 J. Chem. Phys. **106** 3159-73.
[5] Assenmacher F, Gutmann M, Hohlneicher G, Stert V, and Radloff W 2001 Phys. Chem. Chem. Phys. **3** 2981-2.
[6] Fuß W, Schmid W E, and Trushin S A 2001 Chem. Phys. Lett. **342** 91-8.
[7] Robinson J C, Harris S A, Sun W, Sveum N E, and Neumark D M 2002 J. Am. Chem. Soc. **124** 10211-24.
[8] Mu X, Lu I-C, Lee S-H, Wang X, and Yang X 2004 J. Phys. Chem. A **108** 11470-6.
[9] Deleuze M S and Knippenberg S 2006 J. Chem. Phys. **125** 104309.
[10] Levine B G and Martínez T J 2009 J. Phys. Chem. A **113** 12815-24.
[11] Boguslavskiy A E, Mikosch J, Gijsbertsen A, Spanner M, Patchkovskii S, Gador N, Vrakking M J J, and Stolow A 2012 Science **335** 1336-40
[12] Schalk O, Boguslavskiy A E, and Stolow A 2014 J. Phys. Chem. Lett. **5** 560-5.
[13] Makida A, Igarashi H, Fujiwara T, Sekikawa T, Harabuchi Y, and Taketsugu T 2014 J. Phys. Chem. Lett. **5** 1760-5.
[14] Fahr A and Nayak A K 1994 Chem. Phys. **189** 725-31.
[15] Leopold D G, Pendley R D, Roebber J L, Hemley R J, and Vaida V 1984 J. Chem. Phys. **81** 4218-29.
[16] Sekikawa T, Kobayashi T, and Inabe T 1997 J. Phys. Chem. A **101** 644-9.

[17] Sekikawa T, Kobayashi T, and Inabe T 1997 J. Phys. Chem. B **101** 10645-52.
[18] Sekikawa T, Schalk O, Wu G, Boguslavskiy A E, and Stolow A 2013 J. Phys. Chem. A **117** 2971-9.
[19] Pauling L, *The nature of the chemical bond and the strucutre of molecules and crystals: An intorduction to modern structural chemistry* (Cornell university press, Ithaca, New York, 1960), Third edn.
[20] Ichikawa H and Takatsuka K 2017 J. Phys. Chem. A **121** 315-25.
[21] Igarashi H, Makida A, Ito M, and Sekikawa T 2012 Opt. Express **20** 3725–32.
[22] Ito M, Kataoka Y, Okamoto T, Yamashita M, and Sekikawa T 2010 Opt. Express **18** 6071-8.
[23] Iikubo R, Sekikawa T, Harabuchi Y, and Taketsugu T 2016 Faraday Discuss. **194** 147-60.
[24] Villoresi P 1999 Appl. Opt. **38** 6040-9.
[25] Poletto L, Villoresi P, Benedetti E, Ferrari F, Stagira S, Sansone G, and Nisoli M 2007 Opt. Lett. **32** 2897-9.
[26] Biswas S, Förg B, Ortmann L, Schötz J, Schweinberger W, Zimmermann T, Pi L, Baykusheva D, Masood H A, Liontos I, Kamal A M, Kling N G, Alharbi A F, Alharbi M, Azzeer A M, Hartmann G, Wörner H J, Landsman A S, and Kling M F 2020 Nat. Phys. **16** 778–83.
[27] Glover T E, Schoenlein R W, Chin A H, and Shank C V 1996 Phys. Rev. Lett. **76** 2468-71.
[28] Werner H-J 2010 Mol. Phys. **89** 645-61.
[29] Harabuchi Y, Maeda S, Taketsugu T, Minezawa N, and Morokuma K 2013 J. Chem. Theory Comput. **9** 4116–23.
[30] Shao Y and Head-Gordon M 2003 J. Chem. Phys. **118** 4807-18.
[31] Harabuchi Y, Taketsugu T, and Maeda S 2017 Chem. Phys. Lett. **674** 141-5.
[32] Bearpark M J, Robb M A, and Schlegel H B 1994 Chem. Phys. Lett. **223** 269-74.
[33] Maeda S, Ohno K, and Morokuma K 2010 J. Chem. Theory Comput. **6** 1538-45.
[34] Sicilia F, Blancafort L, Bearpark M J, and Robb M A 2008 J. Chem. Theory Comput. **4** 257-66.
[35] Maeda S, Harabuchi Y, Takagi M, Saita K, Suzuki K, Ichino T, Sumiya Y, Sugiyama K, and Ono Y 2018 J. Comp. Chem. **39** 233-51.
[36] Gordon M S and Schmidt M W, in *Theory and Applications of Computational Chemistry, the first forty years*, edited by C. E. Dykstra, G. Frenking, K. S. Kim, and G. E. Scuseria (Elsevier, Amsterdam, 2005), pp. 1167-89.
[37] Werner H-J, Knowles P J, Knizia G, Manby F R, Schütz M, Celani P, Korona T, Lindh R, Mitrushenkov A, Rauhut G, Shamasundar K R, Adler T B, Amos R D, Bernhardsson A, Berning A, Cooper D L, Deegan M J O, Dobbyn A J, Eckert F, Goll E, Hampel C, Hesselmann A, Hetzer G, Hrenar T, Jansen G, Köppl C, Liu Y, Lloyd A W, Mata R A, May A J, Mcnicholas S J, Meyer W, Mura M E, Nicklass A, O'neill D P, Palmieri P, Peng D, Pflüger K, Pitzer R, Reiher M, Shiozaki T, Stoll H, Stone A J, Tarroni R, Thorsteinsson T, and Wang M, MOLPRO, version 2012.1, a package of *ab inito* programs, see http://www.molpro.net.
[38] Knowles P J and Werner H-J 1985 Chem. Phys. Lett. **115** 259-67.
[39] Werner H-J and Knowles P J 1985 J. Chem. Phys. **82** 5053-63.
[40] Iikubo R, Fujiwara T, Sekikawa T, Harabuchi Y, Satoh S, Taketsugu T, and Kayanuma Y 2015 J. Phys. Chem. Lett. **6** 2463-8.
[41] Kobayashi Y, Chang K F, Poullain S M, Scutelnic V, Zeng T, Neumark D M, and Leone S R 2020 Phys. Rev. A **101** 063414.
[42] Adachi S, Kobryanskii V M, and Kobayashi T 2002 Phys. Rev. Lett. **89** 027401.
[43] Tretiak S, Saxena A, Martin R L, and Bishop A R 2003 Proc. Natl. Acad. Sci. USA **100** 2185-90.